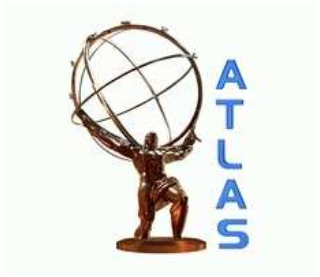

ATLAS NOTE

ATL-PHYS-PUB-2009-004

April 26, 2009

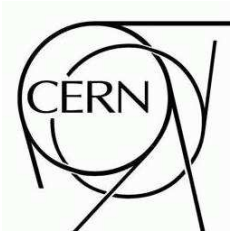

Reconstruction and Identification of Electrons

The ATLAS Collaboration[1)]

This note is part of CERN-OPEN-2008-020. This version of the note should not be cited: all citations should be to CERN-OPEN-2008-020.

[1)]This note prepared by M. Aharrouche, A. Ahmad, C. Anastopoulos, X. Anduaga, O. Arnaez, J.T. Baines, D. Banfi, K. Benslama, R.E. Blair, E.V. Bouhova-Thacker, C. Bourdarios, L. Carminati, J. Cochran, T. Cornelissen, R. Coura Torres, D. Damazio, A. De Santo, J. Del Peso, F. Derue, L. Di Ciaccio, K. Dindar, E. Dobson, M. Donega, M.T. Dova, M. Elsing, D. Emeliyanov, D. Enoque Ferreira de Lima, Y. Fang, O.L. Fedin, M. Fiascaris, H. Flacher, L.R. Flores Castillo, M.J. Flowerdew, T.M. Fonseca Martin, D. Froidevaux, O. Gaumer, I.L. Gavrilenko, R. Gonçalo, G. Gorfine, C. Goy, I. Grabowska-Bold, K. Grimm, H.K. Hadavand, J. Haller, M. Hance, J. Hoffman, T. Hryn'ova, D. Joffe, A. Kaczmarska, V. Kartvelishvili, A. Kasmi, R. Kehoe, N. Kerschen, G. Khoriauli, G. Kilvington, H. Kim, J. Kirk, G.P. Kirsch, K. Koeneke, T. Koffas, I. Koletsou, N. Konstantinidis, V.V. Kostyukhin, S. Laplace, F. Ledroit-Guillon, J.S.H. Lee, D. Lelas, T. Lenz, Z. Liang, W. Liebig, M. Losada, I. Ludwig, E. Lytken, H. Ma, N. Makovec, V.P. Maleev, L. Mandelli, J.-F. Marchand, F.F. Martin, S. Mättig, B.R. Mellado Garcia, F. Monticelli, D. Moreno, A.K. Morley, E.J.W. Moyse, G.A. Navarro, E. Nebot, C. Nelson, V.E. Ozcan, E. Paganis, F. Parodi, J. Parsons, V. Perez Reale, T.C. Petersen, G. Pinzon, A. Poppleton, K. Prokofiev, S. Rajagopalan, I. Riu Dachs, D. Rodriguez, Y. Rodriguez, S. Rosati, D. Rousseau, A. Salzburger, H. Sandaker, C. Santamarina Rios, C. Schiavi, C. Schmitt, S. Sivoklokov, S. Snyder, M.R. Sutton, M.C. Tamsett, J. Tojo, M.F. Tripiana, V. Tsulaia, E. Turlay, G. Unal, M. Wang, A.T. Watson, A.R. Weidberg, M. Wielers, A. Wildauer, E. Woehrling, X. Wu, J. Yu, D. Zerwas, N. Zhou, and H.Z. Zhu.

Abstract

This note discusses the overall ATLAS detector performance for the reconstruction and identification of high-p_T electrons over a wide range of transverse energies, spanning from 10 GeV to 1000 GeV.

Electrons are reconstructed using information from both the calorimeter and the inner detector. The reference offline performance in terms of efficiencies for electrons from various sources and of rejections against jets is described. In a second part, this note discusses the requirements and prospects for electrons as probes for physics within and beyond the Standard Model: Higgs-boson, supersymmetry and exotic scenarios. In the last part, this note outlines prospects for electron identification with early data, corresponding to an integrated luminosity of 100 pb^{-1} , focusing on the use of the signal from $Z \rightarrow ee$ decays for a data-driven evaluation of the offline performance.

1 Introduction

Excellent particle identification capability is required at the LHC for most physics studies. Several channels expected from new physics, for instance some decay modes of the Higgs boson into electrons, have small cross-sections and suffer from large (usually QCD) backgrounds. Therefore powerful and efficient electron identification is needed to observe such signals. Even for standard processes, the signal-to-background ratio is usually less favourable than at past and present hadron colliders. The ratio between the rates of isolated electrons and the rate of QCD jets with p_T in the range 20-50 GeV is expected to be $\sim 10^{-5}$ at the LHC, almost two orders of magnitude smaller than at the Tevatron $p\bar{p}$ collider. Therefore, to achieve comparable performances, the electron identification capability of the LHC detectors must be almost two orders of magnitude better than what has been achieved so far.

Physics channels of prime interest at the LHC are expected to produce electrons with p_T between a few GeV and 5 TeV. Good electron identification is therefore needed over a broad energy range. In the moderate p_T region (20 - 50 GeV), a jet-rejection factor exceeding 10^5 will be needed to extract a relatively pure inclusive signal from genuine electrons above the residual background from jets faking electrons. The required rejection factor decreases rapidly with increasing p_T to $\sim 10^3$ for jets in the TeV region. For multi-lepton final states, such as possible $H \rightarrow eeee$ in the mass region $130 < m_H < 180$ GeV, a rejection of ~ 3000 per jet should be sufficient to reduce the fake-electron backgrounds to a level well below that from real electrons. In this case, however, the electrons have a rather soft p_T spectrum (as low as 5 GeV), resulting in lower reconstruction and identification efficiencies.

Since the publication of the ATLAS physics TDR [1], the ATLAS detector description has been greatly improved, with, in particular, the introduction of a more realistic material description for the inner detector and for the region between the inner detector and the first layer of the electromagnetic calorimeter [2] [3]. This has led to some significant changes in the expected performance. The reconstruction software has also evolved significantly. Each step of the energy reconstruction has been validated by a series of beam tests [4] [5] [6] using prototype modules of the liquid argon electromagnetic calorimeter, and also more recently, combined with prototype modules of the inner detector. At present, two electron reconstruction algorithms have been implemented in the ATLAS offline software, both integrated into one single package and a common event data model.

- The standard one, which is seeded from the electromagnetic (EM) calorimeters, starts from clusters reconstructed in the calorimeters and then builds the identification variables based on information from the inner detector and the EM calorimeters.

- A second algorithm, which is seeded from the inner detector tracks, is optimized for electrons with energies as low as a few GeV, and selects good-quality tracks matching a relatively isolated deposition of energy in the EM calorimeters. The identification variables are then calculated in the same way as for the standard algorithm.

The standard algorithm is the one used to obtain the results presented in this note, while the track-based algorithm is used for low p_T and non-isolated electrons and is the subject of another note [7].

This note is organised as follows. Section 2 discusses the reconstruction and identification of electrons in the fiducial range of the ATLAS detector ($|\eta| < 2.5$), whereas section 3 describes the identification of electrons in the forward region ($2.5 < |\eta| < 4.9$). Section 4 describes some important performance aspects of electron identification in discovery physics processes. Section 5 discusses the strategies for measuring reconstruction and identification efficiencies using a data-driven approach based on $Z \rightarrow ee$ events.

2 Calorimeter-seeded reconstruction and identification

In the standard reconstruction of electrons, a seed electromagnetic tower with transverse energy above $\sim$ 3 GeV is taken from the EM calorimeter [3] and a matching track is searched for among all reconstructed tracks which do not belong to a photon-conversion pair reconstructed in the inner detector. The track, after extrapolation to the EM calorimeter, is required to match the cluster within a broad $\Delta\eta \times \Delta\phi$ window of 0.05×0.10. The ratio, E/p, of the energy of the cluster to the momentum of the track is required to be lower than 10. Approximately 93% of true isolated electrons, with $E_T > 20$ GeV and $|\eta| < 2.5$, are selected as electron candidates. The inefficiency is mainly due to the large amount of material in the inner detector and is therefore η-dependent. As an example, 4% of electron candidates with $p_T = 40$ GeV fail the cut $E/p < 10$ and most of the losses are in the end-cap region. Various identification techniques can be applied to the reconstructed electron candidates, combining calorimeter and track quantities and the TRT information to discriminate jets and background electrons from the signal electrons. A simple cut-based identification procedure is described below together with its expected performance. This is followed by a brief overview of the possibilities offered by more advanced methods, such as a likelihood discriminant.

2.1 Electron-jet studies

For the purposes of this note, the electron identification efficiency is defined as

$$\varepsilon = \frac{N_e^{\mathrm{Id}}}{N_e^{\mathrm{truth}}},$$

where N_e^{Id} is the number of reconstructed and identified candidates and N_e^{truth} is the number of true electrons selected using the appropriate kinematic cuts at the generator level. A geometrical matching (within a cone of size $\Delta R = 0.2$) between the reconstructed cluster and the true electron is required in the calculation of N_e^{Id}. A classification is applied to define whether a reconstructed electron candidate should be considered as signal or background. This classification is based on the type of the Monte Carlo particle associated to the reconstructed track, as well as that of its non-electron parent particle. As shown in Table 1, candidates are divided into four categories and signal efficiencies are calculated separately for isolated and non-isolated electrons.

For the jet rejection studies, the PYTHIA (version 6.4) [10] event generator has been used to produce the large statistics of jet background samples required to assess both the trigger and offline performance of the electron reconstruction and identification tools described in this note. Two different samples were generated to cover the E_T -range of interest for single electrons (10-40 GeV). The first one, referred to as filtered di-jets, contains all hard-scattering QCD processes with $E_T > 15$ GeV, e.g. $qg \rightarrow qg$, including heavy-flavour production, together with other physics processes of interest, such as prompt-photon production and single W/Z production. The second one, referred to as minimum bias, contains the same processes without any explicit hard-scattering cut-off. A filter was applied at the generator level to simulate the L1 trigger requirements [11], with the goal of increasing in an unbiased way the probability that the selected jets pass the electron identification cuts after GEANT [12] simulation. The summed transverse energy of all stable particles (excluding muons and neutrinos) with $|\eta| < 2.7$ in a region $\Delta\phi \times \Delta\eta = 0.12 \times 0.12$ was required to be greater than a chosen E_T -threshold for an event to be retained. For the filtered di-jet sample, this E_T -threshold is 17 GeV, while for the minimum-bias sample, it is 6 GeV. The filter retains 8.3% of the di-jet events and 5.7% of the minimum-bias events. The total number of events available for analysis after filtering, simulation and reconstruction, amounts to 8.2 million events for the di-jet sample and to 4.1 million events for the minimum-bias sample.

The jet rejections quoted in this note are normalised with respect to the number of particle jets reconstructed using particle four-momenta within a cone size $\Delta R = 0.4$ and derived from a dedicated

Category	Type of particle	Type of parent particle
Isolated	Electron	Z, W, t, τ or μ
Non-isolated	Electron	J/ψ, b-hadron or c-hadron decays
Background electron	Electron	Photon (conversions), π^0/η Dalitz decays, $u/d/s$-hadron decays
Non-electron	Charged hadrons, μ	

Table 1: Classification of simulated electron candidates according to their associated parent particle. Muons are included as source because of the potential emission of a Bremsstrahlungs photon.

$E_T > 17$ GeV			$E_T > 8$ GeV	
Isolated	Non-isolated	Background	Non-isolated	Background
W – 75.0%	b-hadrons – 38.7%	γ-conv. – 97.8%	b-hadrons – 39.3%	γ-conv. – 98.4%
Z – 20.9%	c-hadrons – 60.6%	Dalitz decays – 1.8%	c-hadrons – 59.7%	Dalitz decays – 1.3%
t – $< 0.1\%$	J/ψ – 0.7%	$u/d/s$-hadrons – 0.4%	J/ψ – 1.0%	$u/d/s$-hadrons – 0.3%
τ – 4.1%				

Table 2: Contribution and origin of isolated, non-isolated, and background electron candidates in the two di-jet samples before the identification criteria are applied.

un-filtered generated sample of di-jets or minimum-bias events. In the di-jet and minimum-bias samples, the average numbers per generated event of such particle jets with E_T above 17 and 8 GeV, respectively, and in the range $|\eta| < 2.47$, are 0.74 and 0.31, respectively.

After reconstruction of electron candidates and before any of the identification cuts are applied, the signal is completely dominated by non-isolated electrons from $b-$ and c-hadron decays. The expected signal-to-background ratios for the filtered di-jet (E_T above 17 GeV) and minimum-bias (E_T above 8 GeV) samples are 1:80 and 1:50, respectively. The residual jet background is dominated by charged hadrons. Only a small fraction of the background at this stage consists of electrons from photon conversions or Dalitz decays, namely 6.4% and 9.4%, respectively. Table 2 summarises the relative compositions of the filtered di-jet and minimum-bias samples in terms of the three categories containing electrons described in Table 1.

2.1.1 Cut-based method description

Standard identification of high-p_T electrons is based on many cuts which can all be applied independently. These cuts have been optimised in up to seven bins in η and up to six bins in p_T . Three reference sets of cuts have been defined: loose, medium and tight, as summarised in Table 3. This provides flexibility in analysis, for example to improve the signal efficiency for rare processes which are not subject to large backgrounds from fakes.

2.1.1.1 Loose cuts This set of cuts performs a simple electron identification based only on limited information from the calorimeters. Cuts are applied on the hadronic leakage and on shower-shape variables, derived from only the middle layer of the EM calorimeter (lateral shower shape and lateral shower width). This set of cuts provides excellent identification efficiency, but low background rejection.

2.1.1.2 Medium cuts This set of cuts improves the quality by adding cuts on the strips in the first layer of the EM calorimeter and on the tracking variables:

- Strip-based cuts are effective in the rejection of $\pi^0 \to \gamma\gamma$ decays. Since the energy-deposit pattern from π^0's is often found to have two maxima due to $\pi^0 \to \gamma\gamma$ decay, showers are studied in a

Type	Description	Variable name
Loose cuts		
Acceptance of the detector	$\lvert\eta\rvert < 2.47$	
Hadronic leakage	Ratio of E_T in the first sampling of the hadronic calorimeter to E_T of the EM cluster	
Second layer of EM calorimeter.	Ratio in η of cell energies in 3×7 versus 7×7 cells.	R_η
	Ratio in ϕ of cell energies in 3×3 versus 3×7 cells.	R_ϕ
	Lateral width of the shower.	
Medium cuts (includes loose cuts)		
First layer of EM calorimeter.	Difference between energy associated with the second largest energy deposit and energy associated with the minimal value between the first and second maxima.	ΔE_s
	Second largest energy deposit normalised to the cluster energy.	R_{max2}
	Total shower width.	w_{stot}
	Shower width for three strips around maximum strip.	w_{s3}
	Fraction of energy outside core of three central strips but within seven strips.	F_{side}
Track quality	Number of hits in the pixel detector (at least one).	
	Number of hits in the pixels and SCT (at least nine).	
	Transverse impact parameter ($<$1 mm).	
Tight (isol) (includes medium cuts)		
Isolation	Ratio of transverse energy in a cone $\Delta R < 0.2$ to the total cluster transverse energy.	
Vertexing-layer	Number of hits in the vertexing-layer (at least one).	
Track matching	$\Delta\eta$ between the cluster and the track (< 0.005).	
	$\Delta\phi$ between the cluster and the track (< 0.02).	
	Ratio of the cluster energy to the track momentum.	E/p
TRT	Total number of hits in the TRT.	
	Ratio of the number of high-threshold hits to the total number of hits in the TRT.	
Tight (TRT) (includes tight (isol) except for isolation)		
TRT	Same as TRT cuts above, but with tighter values corresponding to about 90% efficiency for isolated electrons.	

Table 3: Definition of variables used for loose, medium and tight electron identification cuts. The cut values are given explicitly only when they are independent of η and p_T . For a detailed description of the cut variables used for the loose and medium cuts, refer to sections 2.1.1.1 and 2.1.1.2.

window $\Delta\eta \times \Delta\phi = 0.125 \times 0.2$ around the cell with the highest E_T to look for a second maximum. If more than two maxima are found the second highest maximum is considered. The variables used include $\Delta E_s = E_{\mathrm{max2}} - E_{\mathrm{min}}$, the difference between the energy associated with the second maximum E_{max2} and the energy reconstructed in the strip with the minimal value, found between the first and second maxima, E_{min}. Also included are: $R_{\mathrm{max2}} = E_{\mathrm{max2}}/(1+9\times10^{-3}E_T)$, where E_T is the transverse energy of the cluster in the EM calorimeter and the constant value 9 is in units of GeV^{-1}; w_{stot}, the shower width over the strips covering 2.5 cells of the second layer (20 strips in the barrel for instance); w_{s3}, the shower width over three strips around the one with the maximal energy deposit; and F_{side}, the fraction of energy deposited outside the shower core of three central strips.

- The tracking variables include the number of hits in the pixels, the number of silicon hits (pixels plus SCT) and the tranverse impact parameter.

The medium cuts increase the jet rejection by a factor of 3-4 with respect to the loose cuts, while reducing the identification efficiency by $\sim 10\%$.

2.1.1.3 Tight cuts This set of cuts makes use of all the particle-identification tools currently available for electrons. In addition to the cuts used in the medium set, cuts are applied on the number of vertexing-layer hits (to reject electrons from conversions), on the number of hits in the TRT, on the ratio of high-threshold hits to the number of hits in the TRT (to reject the dominant background from charged hadrons), on the difference between the cluster and the extrapolated track positions in η and ϕ, and on the ratio of cluster energy to track momentum, as shown in Table 3. Two different final selections are available within this tight category: they are named tight (isol) and tight (TRT) and are optimised differently for isolated and non-isolated electrons. In the case of tight (isol) cuts, an additional energy isolation cut is applied to the cluster, using all cell energies within a cone of $\Delta R < 0.2$ around the electron candidate. This set of cuts provides, in general, the highest isolated electron identification and the highest rejection against jets. The tight (TRT) cuts do not include the additional explicit energy isolation cut, but instead apply tighter cuts on the TRT information to further remove the background from charged hadrons.

Figures 1 and 2 compare the distributions expected from $Z \rightarrow ee$ decays and from the filtered di-jet sample for a few examples of the basic discriminating variables described above for electron identification.

2.1.2 Performance of cut-based electron identification

The performance of the cut-based electron identification is summarised in Tables 4 and 5. Table 4 shows, for each of the background samples, the composition of each of the three categories of electron candidates containing real electrons, as it evolves from reconstruction (no identification cuts) to loose, medium and tight cuts. In the case of non-isolated electrons, there is a strong reduction of the initially dominant component from c-hadrons as the identification cuts applied become tighter. In the case of background electrons, there is a significant reduction of the contribution from photon conversions when applying tight cuts, since the vertexing-layer requirement does not much affect electrons from Dalitz decays and $u/d/s$-hadrons. As shown in Table 5, the signal from prompt electrons is dominated by non-isolated electrons from heavy flavours, which are usually close in space to hadrons from the jet fragmentation. The resulting overlap between the electron shower and nearby hadronic showers explains the much lower efficiency observed for these electrons than for isolated electrons from $Z \rightarrow ee$ decays. These non-isolated electrons will nevertheless provide the most abundant initial source of signal electrons and will be used for alignment of the electromagnetic calorimeters and the inner detector, for E/p calibrations, and more generally to improve the understanding of the material of the inner detector as a radiation/conversion

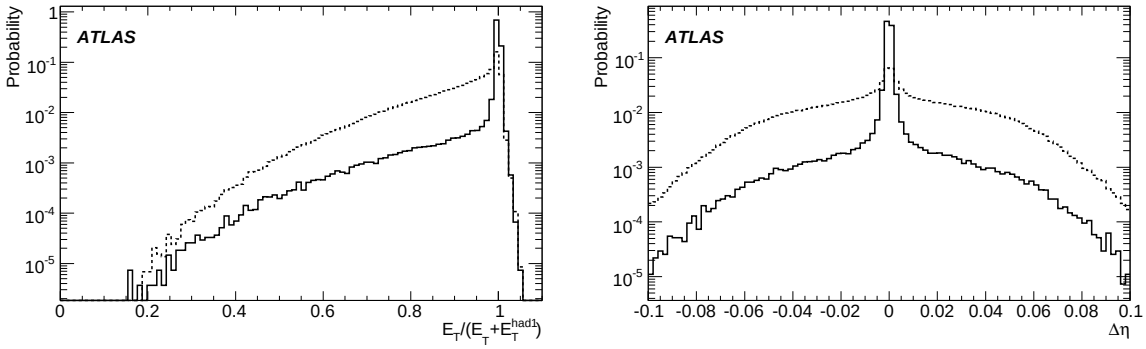

Figure 1: Left: ratio between the transverse energy of the electron candidate and the sum of this transverse energy and that contained in the first layer of the hadronic calorimeter. The distributions are shown for electrons from $Z \rightarrow ee$ decays (solid line) and for filtered di-jets (dotted line). Right: difference in η between cluster and extrapolated track positions for electrons from $Z \rightarrow ee$ decays (solid line) and for filtered di-jets (dotted line).

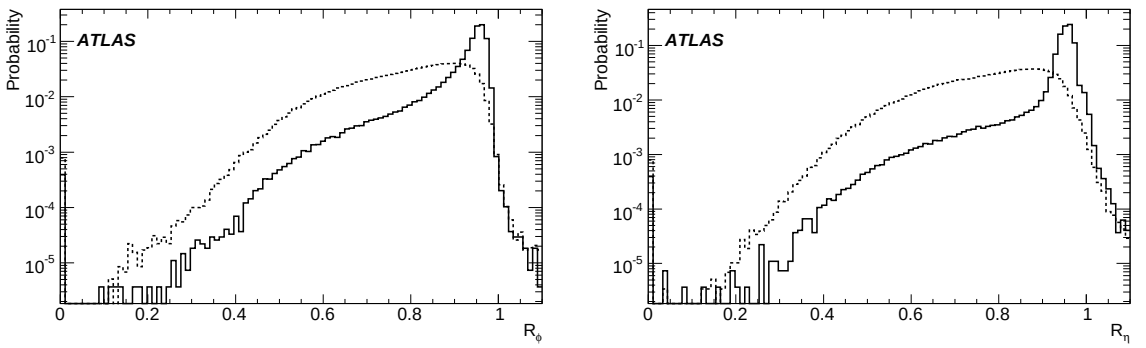

Figure 2: Shower-shape distributions for electrons from $Z \rightarrow ee$ decays (solid lines) compared to those from filtered di-jets (dotted lines). Shown are the energy ratios R_ϕ (left) and R_η (right) described in Table 3.

source. For tight cuts and an electron E_T of $\sim$ 20 GeV, the isolated electrons from W, Z and top-quark decays represent less than 20% of the total prompt electron signal.

For the lower E_T -threshold of 8 GeV, the expected signal from isolated electrons is negligible. Not surprisingly, the tight (TRT) cuts are more efficient to select non-isolated electrons from heavy-flavour decay, while the tight (isol) cuts are more efficient at selecting isolated electrons. After tight cuts, the signal-to-background ratio is close to 3:1, and depends only weakly on the E_T - threshold in the 10-40 GeV E_T -range studied here. The residual background is dominated by charged hadrons, which could be further rejected by stronger cuts (TRT and/or isolation). The initial goal of obtaining a rejection of the order of 10^5 against jets has been achieved with an overall efficiency of 64% for isolated electrons with $E_T \sim$ 10-40 GeV. The efficiency may be improved with further optimisation of the cuts, as discussed below.

Table 6 shows the efficiencies for prompt electrons and the jet rejections in more detail in the case of medium identification cuts, using a fine binning as a function of $|\eta|$. The efficiency for prompt electrons is significantly worse in the end-cap region ($|\eta| > 1.52$) with a correspondingly higher background

Isolated										
	$E_T > 17$ GeV									
	No cut		Loose		Medium	Tight (TRT)			Tight (isol)	
W	75.0		75.1		74.9	73.9			73.6	
Z	20.9		20.9		21.1	22.4			22.9	
τ	4.1		4.0		4.0	3.7			3.6	
Non-isolated										
	$E_T > 17$ GeV					$E_T > 8$ GeV				
	No cut	Loose	Medium	Tight (TRT)	Tight (isol)	No cut	Loose	Medium	Tight (TRT)	Tight (isol)
b-hadrons	38.7	57.6	71.1	74.2	79.1	39.3	51.2	55.2	57.0	59.5
c-hadrons	60.6	41.4	27.6	24.4	19.6	59.7	47.6	43.2	41.3	38.6
J/ψ	0.7	1.0	1.3	1.4	1.3	1.0	1.2	1.6	1.7	1.9
Background										
	$E_T > 17$ GeV					$E_T > 8$ GeV				
	No cut	Loose	Medium	Tight (TRT)	Tight (isol)	No cut	Loose	Medium	Tight (TRT)	Tight (isol)
γ-conv.	97.8	97.7	94.9	88.0	88.1	98.4	98.1	94.5	78.5	83.0
Dalitz decays	1.8	1.9	4.0	8.5	8.0	1.3	1.4	3.5	12.5	12.4
$u/d/s$-hadrons	0.4	0.4	1.1	3.5	3.9	0.3	0.5	2.0	9.0	4.6

Table 4: Percentage contribution and origin of isolated, non-isolated and background electrons in the filtered di-jet and minimum-bias samples. The classification is based on the type of the parent particle of the electron.

rejection. The overlap region region between the barrel and end-cap calorimeters ($1.37 < |\eta| < 1.52$) has both worse efficiency and rejection, as expected because of the large amount of passive material in front of the EM calorimeter. To improve the electron efficiency in the end-cap region, the EM calorimeter cuts in the first layer and the tracking cuts will need to be studied and tuned further.

2.1.3 Expected differential rates for inclusive electron signal and background

Figure 3 (left: $E_T > 17$ GeV and right: $E_T > 8$ GeV) show the expected differential cross-sections for electron candidates as a function of E_T, for an integrated luminosity of 100 pb^{-1}. The different histograms correspond to electron candidates before any identification cuts and after the loose, medium, tight (TRT) and tight (isol) cuts. As illustrated in Table 5, these differential rates are dominated by the jet background except when applying the tight cuts.

The expected differential cross-sections after tight (TRT) cuts are shown in Fig. 4, where they are broken down into their three main components, isolated electrons from W, Z and top-quark decays, non-isolated electrons from b, c decay, and the residual jet background. The shapes of the spectra for the non-isolated electrons and residual jet background are very similar, whereas the spectrum from isolated electrons exhibits the expected behaviour for a sample dominated by electrons from W, Z decay. For an integrated luminosity of 100 pb^{-1}, Fig. 4 (right) shows that one may expect approximately ten million reconstructed and identified inclusive electrons from b, c decay with $E_T > 10$ GeV, while Fig. 4 (left) shows that for the same integrated luminosity one may expect 500 000 such electrons with $E_T > 20$ GeV, with a dominant contribution from W, Z decays for $E_T > 35$ GeV. These large data samples expected for a modest integrated luminosity are an integral part of the trigger menu strategy for early data, as explained in more detail in [11], and will clearly be extremely useful to certify many aspects of the electron identification performance of ATLAS with real data. One example is the understanding of material effects and of inter-calibration between inner detector and EM calorimeter using E/p for a clean subset of the inclusive electrons with $E_T > 10$ GeV. This sample will be complementary to the samples of low-mass electron pairs from J/ψ and Υ decays, discussed in [7]. A second example is the certification of the isolated electron identification using a clean sample of $W \rightarrow e\nu$ decays. Clearly,

Cuts	E_T > 17 GeV			E_T > 8 GeV		
	Efficiency (%)		Jet rejection	Efficiency (%)		Jet rejection
	$Z \rightarrow ee$	$b,c \rightarrow e$		Single electrons (E_T =10 GeV)	$b,c \rightarrow e$	
Loose	87.96 ± 0.07	50.8 ± 0.5	567 ± 1	75.8 ± 0.1	55.8 ± 0.7	513 ± 2
Medium	77.29 ± 0.06	30.7 ± 0.5	2184 ± 13	64.8 ± 0.1	41.9 ± 0.7	1288 ± 10
Tight (TRT.)	61.66 ± 0.07	22.5 ± 0.4	$(8.9 \pm 0.3)10^4$	46.2 ± 0.1	29.2 ± 0.6	$(6.5 \pm 0.3)10^4$
Tight (isol.)	64.22 ± 0.07	17.3 ± 0.4	$(9.8 \pm 0.4)10^4$	48.5 ± 0.1	28.0 ± 0.6	$(5.8 \pm 0.3)10^4$
	Fraction of surviving candidates (%)			Fraction of surviving candidates (%)		
	Isolated	Non-isolated	Jets	Non-isolated		Jets
Medium	1.1	7.4	91.5 (5.5 + 86.0)	9.0		91.0 (5.0 + 86.0)
Tight (TRT)	10.5	63.3	26.2 (8.3 + 17.9)	77.8		22.2 (7.1 + 15.1)
Tight (isol)	13.0	58.3	28.6 (8.7 + 19.9)	75.1		24.9 (6.4 + 18.5)

Table 5: Expected efficiencies for isolated and non-isolated electrons and corresponding jet background rejections for the four standard levels of cuts used for electron identification. The results are shown for the simulated filtered di-jet and minimum-bias samples, corresponding respectively to E_T -thresholds of 17 GeV (left) and 8 GeV (right). The three bottom rows show the fractions of all surviving candidates which fall into the different categories for the medium cuts and the two sets of tight cuts. The isolated electrons are prompt electrons from W, Z and top-quark decay and the non-isolated electrons are from b, c decay. The residual jet background is split into its two dominant components, electrons from photon conversions and Dalitz decays (first term in brackets) and charged hadrons (second term in brackets). The quoted errors are statistical.

with more statistics, the large samples of $Z \rightarrow ee$ decays which will be collected will provide the opportunity to refine the understanding of the performance to an extremely high level of accuracy, as discussed in Section 5.

2.1.4 Systematic uncertainties on expected performance

To estimate possible systematic uncertainties related to the cut-based electron identification, two shower shape variables have been studied as a function of the amount of material in front of the EM calorimeter. Figure 5 illustrates the impact of additional material, the effect of which has not been included in the EM cluster corrections which are applied as described in [3], for electrons from $H \rightarrow eeee$ decays. The results are shown in two $|\eta|$-ranges for the nominal material and for the case of additional material accounting in total to $\sim 0.1\ X_0$ and $\sim 0.2\ X_0$ (Fig. 5). It is evident that in regions with significant amounts of material the shower is broader (less energy in the core). These differences reduce the electron efficiency; however, the true systematic error on the efficiency due to such effects will depend on how well the inner-detector material can be measured using data.

Figure 6 shows the fraction of energy in the strip layer outside the three core strips and inside the seven-strip window for the same $|\eta|$-ranges. The impact of the additional material is also clearly visible. The estimated change in the electron efficiencies quoted in Table 5 is expected to be less than 2%. It is important to note that the material effects are more pronounced in the strip layer than in the middle layer of the calorimeter. Therefore, one should expect larger uncertainties from this source of systematics for the medium electron cuts than for the loose electron cuts, which rely only on the middle layer of the calorimeter.

Another important source of systematics affects the jet rejections quoted in Table 5: this arises from the exact p_T -spectrum and mixture of quark and gluon jets, and to a certain extent from heavy flavour jets present in the background under consideration. The numbers quoted in this note are related to the rather low-p_T di-jet background which is relevant for the search for early signals from single electrons. Other

$\|\eta\|$	$E_T > 17$ GeV			$E_T > 8$ GeV		
	Efficiency (%)		Jet rejection	Efficiency (%)		Jet rejection
	$Z \rightarrow ee$	$b,c \rightarrow e$		Single electrons (E_T =10 GeV)	$b,c \rightarrow e$	
0.00 − 0.80	88.2 ± 0.1	35 ± 1	3740 ± 50	79.3 ± 0.2	51 ± 1	1960 ± 30
0.80 − 1.35	83.5 ± 0.1	40 ± 1	1581 ± 20	70.6 ± 0.2	52 ± 1	914 ± 11
1.35 − 1.50	71.5 ± 0.4	41 ± 2	444 ± 5	49.6 ± 0.5	40 ± 3	342 ± 5
1.50 − 1.80	63.8 ± 0.2	18 ± 1	2440 ± 40	41.8 ± 0.4	24 ± 2	890 ± 15
1.80 − 2.00	62.5 ± 0.2	12 ± 1	9800 ± 450	55.1 ± 0.4	25 ± 2	4660 ± 220
2.00 − 2.35	65.8 ± 0.2	16 ± 1	8400 ± 300	55.0 ± 0.3	21 ± 2	6000 ± 250
2.35 − 2.47	67.8 ± 0.3	14 ± 2	4050 ± 170	62.5 ± 0.6	30 ± 3	3980 ± 250
0.00 − 2.47	77.3 ± 0.06	31 ± 1	2184 ± 13	64.8 ± 0.1	42 ± 1	1288 ± 8

Table 6: Expected efficiencies for isolated and non-isolated electrons and corresponding jet background rejections for the medium identification cuts as a function of $|\eta|$. The results are shown for the simulated filtered di-jet and minimum-bias samples, corresponding respectively to E_T -thresholds of 17 GeV (left) and 8 GeV (right). The quoted errors are statistical.

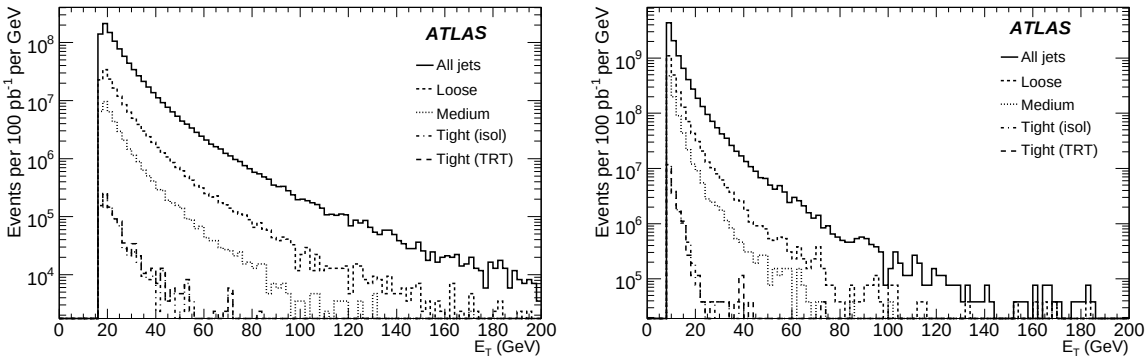

Figure 3: Differential cross-sections as a function of E_T before identification cuts and after loose, medium, tight (TRT) and tight-isol cuts, for an integrated luminosity of 100 pb^{-1} and for the simulated filtered di-jet sample with E_T above 17 GeV (left) and the simulated minimum-bias sample with E_T above 8 GeV (right).

background samples relevant to certain physics studies have been shown to display worse rejections, by up to a factor of 3 to 5. This clearly indicates that the fake electron rates will only be better understood with real data.

2.1.5 Multivariate techniques

In addition to the standard cut-based electron identification described above, several multivariate techniques have been developed and implemented in the ATLAS software. These include a likelihood discriminant, a discriminant called H-matrix, a boosted decision tree, and a neural network. Table 7 summarises the gains in efficiency and rejection which may be expected with respect to the cut-based method by using the likelihood discriminant method. The gains appear to be artificially large in the case of the loose and medium cuts, because these cuts do not make use of all the information available in terms of electron identification, since they were designed for robustness and ease of use with initial data. Nevertheless, they indicate how much the electron efficiency may be improved once all the discriminant

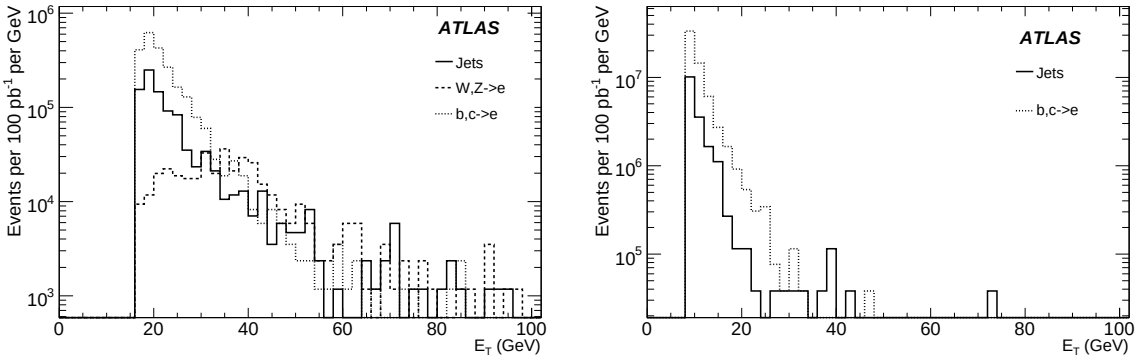

Figure 4: Differential cross-sections as a function of E_T after tight (TRT) cuts, shown separately for the expected components from isolated electrons, non-isolated electrons and residual jet background, for an integrated luminosity of 100 pb^{-1} and for the simulated filtered di-jet sample with E_T above 17 GeV (left) and the simulated minimum-bias sample with E_T above 8 GeV (right).

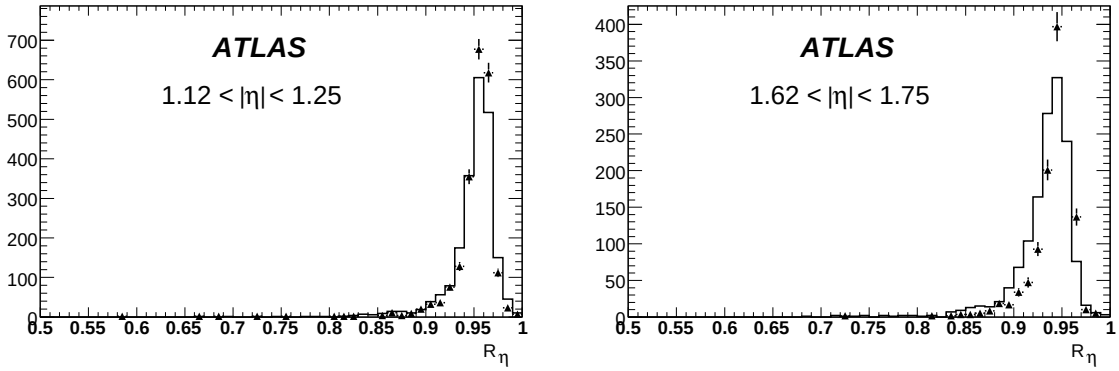

Figure 5: Energy containment, R_η (Table 3), for $1.12 < |\eta| < 1.25$ (left) and $1.62 < |\eta| < 1.75$ (right). The symbols correspond to the nominal description and the histogram to the one with additional material.

variables will be understood in the data.

Figure 7 shows the rejection versus efficiency curve obtained using the likelihood discriminant method, compared to the results obtained for the two sets of tight cuts shown in Table 5. The likelihood discriminant method provides a gain in rejection of about 20-40% with respect to the cut-based method for the same efficiency of 61-64%. Alternatively, it provides a gain in efficiency of 5-10% (tight and medium cuts) for the same rejection. Multivariate methods of this type will of course only be used once the detector performance has been understood using the simpler cut-based electron identification criteria.

2.2 Isolation studies

Many physics analyses in ATLAS will be based on final states with isolated leptons from decays of W- or Z-bosons. These channels usually have the advantage of small background expectation from processes with similar signature, compared to channels with hadronic final states. Nevertheless, they may also suffer from jet background processes, namely if leptons from semi-leptonic heavy-quark decays mimic

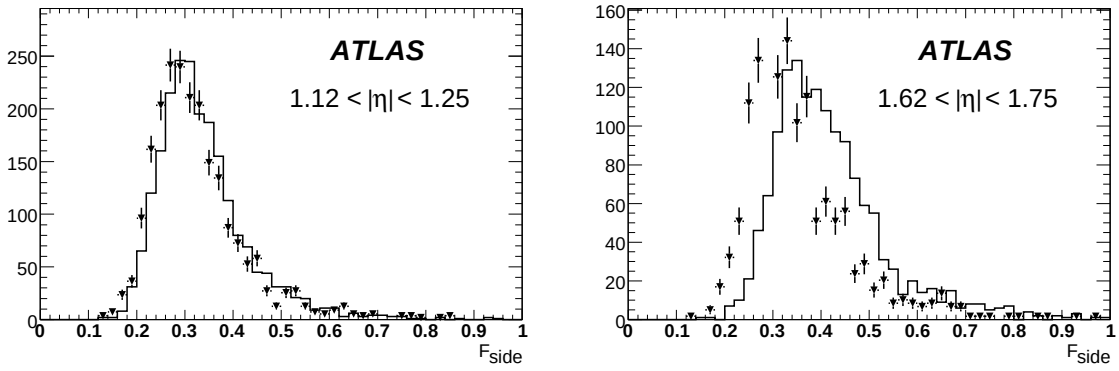

Figure 6: Energy fraction outside a three-strip core, F_{side} (Table 3), for $1.12 < |\eta| < 1.25$ (left) and $1.62 < |\eta| < 1.75$ (right). The symbols correspond to the nominal description and the histogram to the one with additional material.

Cuts	**Cut-based method**		**Likelihood method**	
	Efficiency ε_e (%)	Rejection R_j	Efficiency (%) at fixed R_j	Rejection at fixed ε_e
Loose	87.97 ± 0.05	567 ± 1	89.11 ± 0.05	2767 ± 17
Medium	77.29 ± 0.06	2184 ± 7	88.26 ± 0.05	$(3.77 \pm 0.08) \times 10^4$
Tight (isol)	64.22 ± 0.07	$(9.9 \pm 0.2) \times 10^4$	67.53 ± 0.06	$(1.26 \pm 0.05) \times 10^5$
Tight (TRT)	61.66 ± 0.07	$(8.9 \pm 0.2) \times 10^4$	68.71 ± 0.06	$(1.46 \pm 0.06) \times 10^5$

Table 7: For the loose, medium and tight electron identification cuts, expected electron efficiencies for a fixed jet rejection and jet rejections for a fixed electron efficiency, as obtained from the likelihood discriminant method. The quoted errors are statistical.

the isolated leptons of the signal. Therefore, dedicated tools beyond the lepton identification algorithms are needed in order to suppress such sources of background by factors of up to the order of 10^3. In this section, the performance of a projective likelihood estimator for the separation of isolated electrons from non-isolated electron backgrounds is described. The four variables chosen as input to this isolation likelihood are:

- transverse energy deposited in a small cone of $\Delta R < 0.2$ around the electron cluster;
- transverse energy deposited in a hollow cone of $0.2 < \Delta R < 0.4$ around the electron cluster;
- sum of the squares of the transverse momenta of all additional tracks measured in a cone of $\Delta R < 0.4$ around the electron cluster;
- impact parameter significance of the electron track (with respect to the primary vertex in the transverse plane).

Electrons from $Z \rightarrow ee$ decays were used as a clean source of isolated electrons. The reconstructed electrons from this sample were required to be matched to a Monte Carlo electron from Z-boson decay and to pass the medium identification cuts in order to be considered as signal electrons. Background electrons were selected from a high-statistics $t\bar{t}$ sample, filtered for a pair of like-sign Monte Carlo electrons, and matched to a Monte Carlo electron from b/c-decay.

The results of the performance studies of the isolation likelihood are shown in Fig. 8 for two illustrative bins in $|\eta|$ and p_T . The best results are achieved for high-p_T electrons measured in the barrel

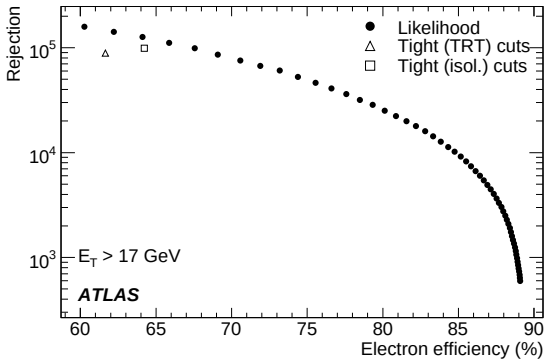

Figure 7: Jet rejection versus isolated electron efficiency obtained with a likelihood method (full circles) compared to the results from the two sets of tight cuts (open triangle and open square).

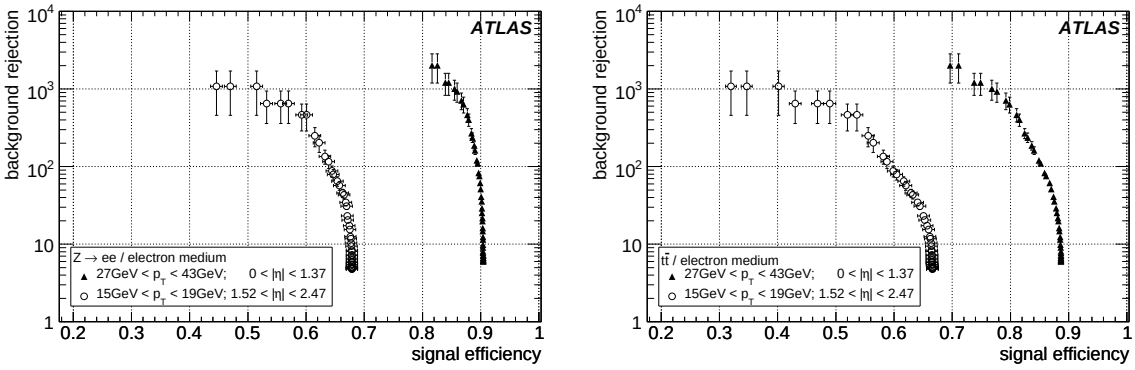

Figure 8: Background electron rejections versus signal efficiencies for electrons in $Z \rightarrow ee$ decays (left) and in $t\bar{t}$ decays (right), for two illustrative bins in $|\eta|$ and p_T .

region of the EM calorimeter. As can be seen in Fig. 8 left, for electrons with only little hadronic activity in the final state, such as those from $Z \rightarrow ee$ and $H \rightarrow eeee$ decays, the isolation likelihood provides a background rejection of the order of 10^3, for signal electron efficiencies of 80% (barrel) and 50% (end-caps). The difference observed between barrel and end-caps is mostly due to the η-dependence of the medium identification cuts shown in Table 6. For comparison, the efficiency for the selection of signal electrons in $t\bar{t}$ events is shown in Fig. 8 right: due to the additional hadronic activity in these final states, the efficiency decreases by 5–10% for the same background rejection, when compared to that quoted for $Z \rightarrow ee$ decays.

3 Electron identification outside the inner detector acceptance

Electron identification in the forward region ($|\eta| > 2.5$) will be important in many physics analyses, including electroweak measurements and searches for new phenomena. In contrast to the central electrons, forward electron reconstruction can only use information from the calorimeters, since the inner detector covers only $|\eta| < 2.5$. Such electrons can therefore only be identified cleanly above the background in specific topologies, such as $Z \rightarrow ee$ or $H \rightarrow eeee$ decays.

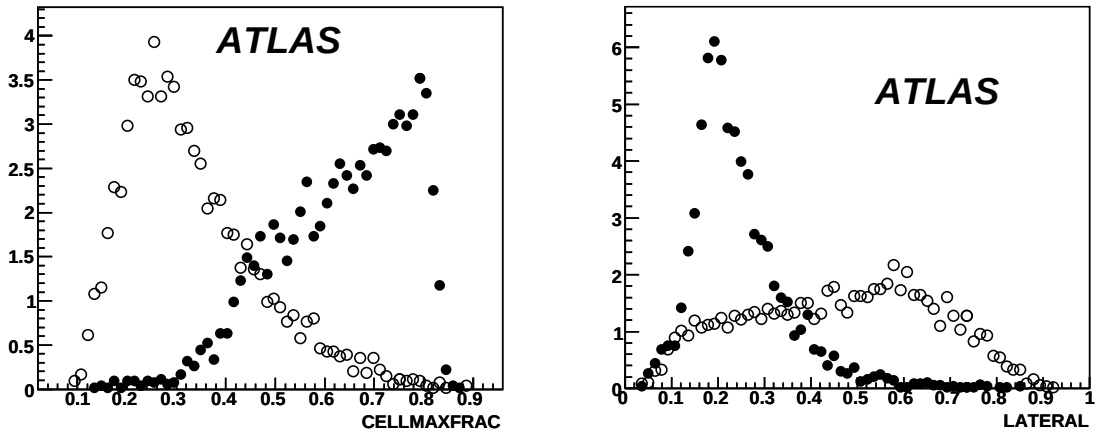

Figure 9: Example of discriminating variables used in the forward region for signal electrons (full circles) and the QCD di-jet background (open circles). Shown in the case of the FCal are the fraction of the total cluster energy deposited in the cell with maximum energy (left) and the relative lateral moment (right).

This section describes the performance of a cut-based method used to identify electrons in the forward region and separate them from the QCD background. The comparison of the performance obtained with a likelihood method is also presented.

Signal electrons are selected from $Z \rightarrow ee$ decays and background electrons from a high-statistics sample of QCD di-jet events. Three $|\eta|$-regions are considered: the first one covers the inner wheel of the electromagnetic end-cap, i.e. $2.5 < |\eta| < 3.2$ (the HEC is not used), the second one covers the overlap region between the electromagnetic end-cap and the forward calorimeter (FCal), i.e. $3.2 < |\eta| < 3.4$, and the last region covers the FCal acceptance, i.e. $3.4 < |\eta| < 4.9$. A topological clustering algorithm [13] is used in this analysis and only clusters with $E_T > 20$ GeV are considered. Two examples of the discriminating variables used in these studies are shown in Fig. 9, namely the fraction of the total cluster energy deposited in the cell with maximum energy and the relative lateral moment. The relative lateral moment is defined as $\mathrm{lat}_2/(\mathrm{lat}_2 + \mathrm{lat}_{\mathrm{max}})$, where the lateral moments lat_2 and $\mathrm{lat}_{\mathrm{max}}$ differ in the treatment of the two most energetic cells. Other examples include the first moment of the energy density, the relative longitudinal moment, defined in the same way as the relative lateral moment only with two longitudinal moments, the second moments of the distances of each cell to the shower barycentre and to the shower axis, and the distance of the cluster barycentre from the front face of the calorimeter.

The likelihood discriminant uses the same variables as the cut-based method. Figure 10 shows the performance of the cut-based and likelihood discriminant methods for electrons from $Z \rightarrow ee$ decay with $E_T > 20$ GeV. For an electron identification efficiency of 80%, both methods achieve the required goal of $\sim 1\%$ fake rate from the QCD background. This performance is expected to yield, for example, a clean $Z \rightarrow ee$ sample with one electron already selected in the central region and one electron in the forward region [14]: the expected background contribution under the Z-boson peak is estimated to be below $\sim$ 1%.

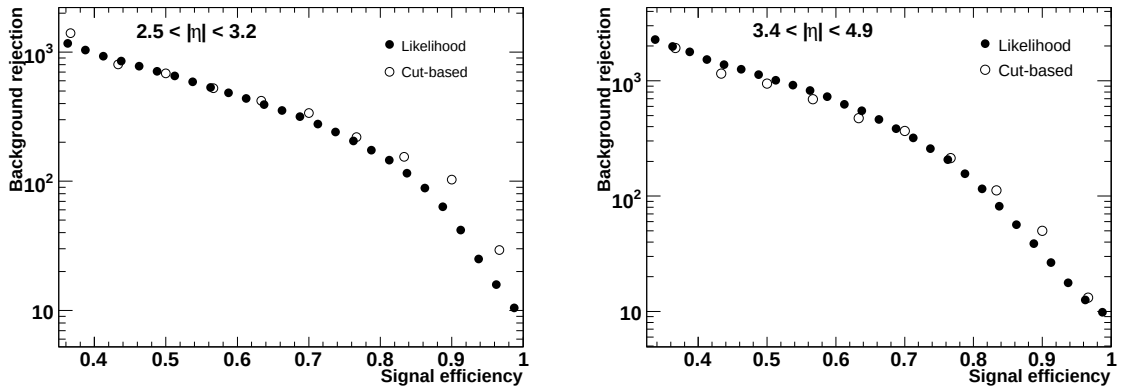

Figure 10: Expected rejection against QCD jets versus efficiency for signal electrons from $Z \rightarrow ee$ decay, for the cut-based and likelihood discriminant methods in the inner wheel of the electromagnetic end-cap (left) and in the FCal (right). The rejection power of the likelihood method is expected to increase when additional variables beyond the minimal set shown here are added.

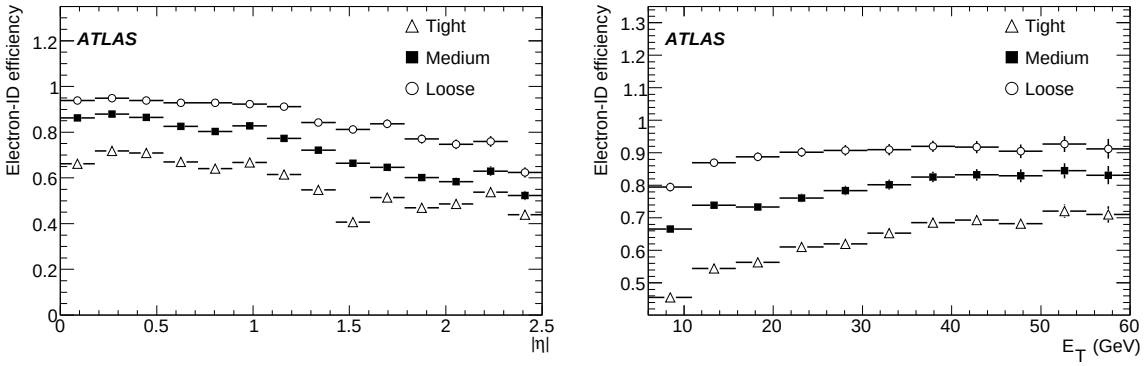

Figure 11: Electron identification efficiency as a function of η (left) and E_T (right) for electrons with $E_T > 5$ GeV from $H \rightarrow eeee$ decays.

4 Electrons as probes for physics within and beyond the Standard Model

4.1 Electrons in Higgs-boson decays

Electrons from the $H \rightarrow eeee$ decay with $m_H < 2m_Z$ are an important benchmark for the evaluation of the performance of the electron reconstruction and identification [15]. Here, only electrons with $|\eta| < 2.5$ and $E_T > 5$ GeV are considered. The electron efficiency as a function of $|\eta|$ and E_T for loose, medium, and tight electron cuts is shown in Fig. 11. The drop in efficiency at low E_T is mainly due to the loss of discrimination power of the shower-shape cuts at lower transverse energies. A loss of efficiency is also visible in the transition region between the barrel and end-cap calorimeters. The results shown here are in quantitative agreement with those obtained for electrons from $Z \rightarrow ee$ decay discussed in Section 2.1.2.

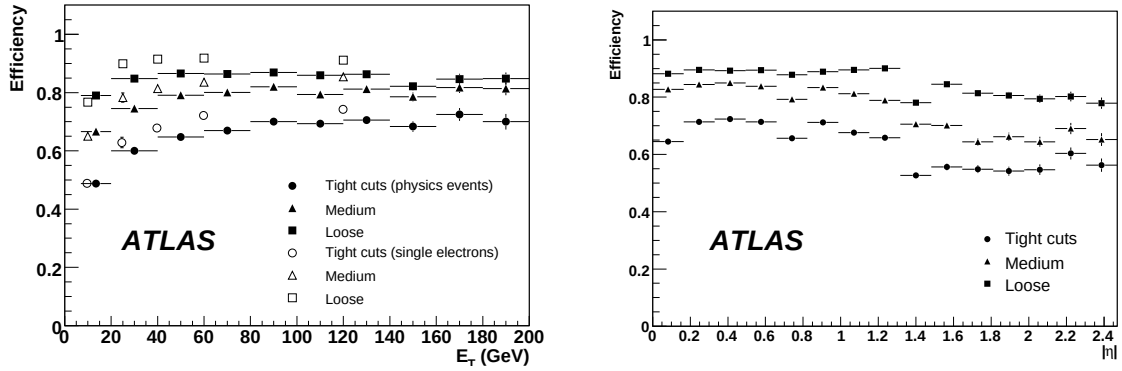

Figure 12: Electron identification efficiency as a function of E_T (left) and $|\eta|$ (right). The full symbols correspond to electrons in SUSY events and the open ones to single electrons of fixed E_T . The efficiencies as a function of $|\eta|$ are shown only for electrons with $E_T > 17$ GeV.

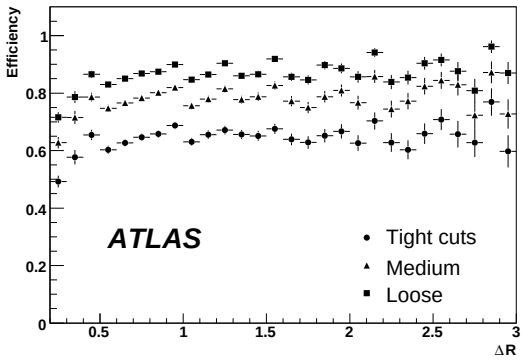

Figure 13: Electron identification efficiency as a function of the distance ΔR to the closest jet in SUSY events, for electrons with $E_T > 17$ GeV.

4.2 Electrons produced in decays of supersymmetric particles

In many supersymmetry (SUSY) scenarios, the most abundantly produced sparticles are squarks (directly or from a gluino decay), which generally decay into a chargino or neutralino and jets. In turn, charginos and neutralinos are very likely to decay into leptons. One interesting mode for SUSY searches is the tri-lepton signal, in which three isolated leptons are expected in the final state. Such SUSY events would feature high-p_T isolated leptons accompanied by a high multiplicity of high-E_T jets. Hence, it is crucial to efficiently identify electrons in such an environment, while preserving the very high jet rejection presented in Section 2. The electron identification efficiency in SUSY events is calculated using the SU3 ATLAS point [16]. In this scenario, a large number of charginos and neutralinos are produced and numerous leptons are expected in the final state.

Figure 12 shows the identification efficiency of the loose, medium and tight (isol) cuts as a function of E_T and $|\eta|$. The efficiencies shown as a function of E_T are compared with efficiencies for single electrons of $E_T = 10$, 25, 40, 60 and 120 GeV. As expected, single electrons display higher efficiencies than those in SUSY events, because of the large hadronic activity in these events. The efficiencies obtained for values of E_T below 20 GeV, are significantly below the plateau values at high E_T , for

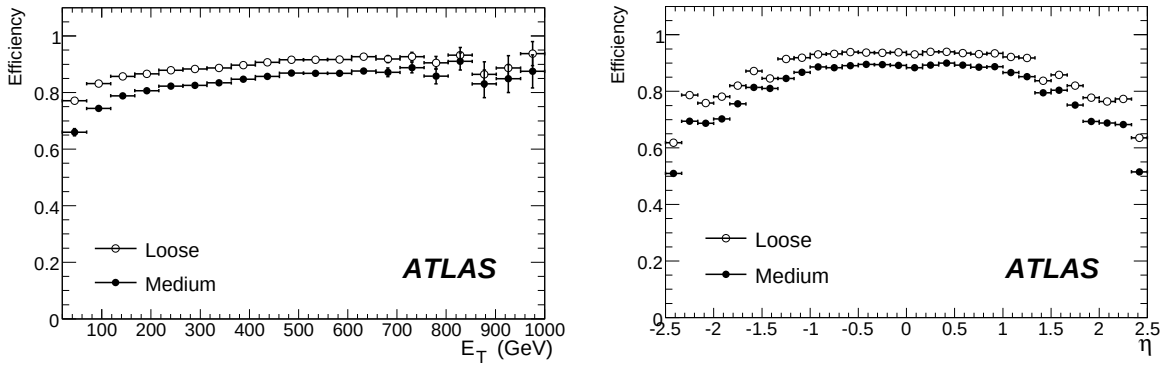

Figure 14: Electron identification efficiency as a function of E_T (left) and $|\eta|$ (right), for electrons from $Z' \to e^+e^-$ decays with $m_{Z'}$ = 1 TeV.

which the cuts were initially optimised.

The efficiencies as a function of $|\eta|$ show the same features as those discussed in Table 6, namely the efficiency in the end-cap region is lower than in the barrel, whereas the jet rejection is significantly higher. Specific drops in efficiency can be seen for $|\eta| \sim 1.35$, which corresponds to the barrel/end-cap transition region, and for $|\eta| \approx 0.8$, which corresponds to the change in the lead thickness between the two types of electrodes in the barrel EM calorimeter.

Figure 13 shows the electron identification efficiency as a function of the distance ΔR to the closest jet in SUSY events. Jets are reconstructed from topological clusters using a $\Delta R = 0.4$ cone algorithm. For values of $\Delta R > 0.4$, the efficiencies are compatible with those expected for single electrons, whereas for values of $\Delta R < 0.4$, the efficiencies decrease because of the overlap between the hadronic showers from the jet and the electron shower itself.

4.3 Electrons in exotic events

High-mass di-electron final states are a promising source of early discovery physics, because of the simplicity and robustness of very high-p_T electron reconstruction, identification and resolution. Very high-p_T electrons refer here to those with transverse momentum ranging from 100 GeV up to several TeV. The backgrounds to very high-p_T electron pairs are expected to be small, and, therefore, only loose or medium identification cuts are considered here. Isolated electrons are required to satisfy the calorimeter isolation cut described in Section 2.

Figure 14 shows efficiencies as a function of E_T and $|\eta|$ for the loose and medium identification cuts, for electrons from $Z' \to e^+e^-$ decays with $m_{Z'}$ = 1 TeV [17]. From these curves, one can note the slow increase in efficiency with E_T before reaching a plateau in the very high-E_T region. Overall efficiencies of $\sim$ 90% and of $\sim$ 85% can be achieved for loose and medium electron cuts, respectively, with a uniform behaviour limited to the barrel region, i.e. $|\eta| < 1.5$.

The QCD background rejection was studied as a function of the jet transverse energy, as shown in Table 8. Using the medium identification cuts, which correspond to an overall efficiency of $\sim$ 85%, a jet rejection factor of several thousand can be achieved for $E_T > 100$ GeV, which should be sufficient to observe the signal in many exotic scenarios.

Jet E_T -range	140 – 280 GeV		280 – 560 GeV		560 – 1120 GeV	
	Efficiency	Rejection	Efficiency	Rejection	Efficiency	Rejection
Loose cuts	$86.6 \pm 0.2\%$	825 ± 35	$89.6 \pm 0.1\%$	620 ± 25	$91.5 \pm 0.4\%$	550 ± 20
Medium cuts	$80.6 \pm 0.2\%$	4000 ± 370	$84.6 \pm 0.1\%$	2300 ± 170	$86.7 \pm 0.5\%$	1900 ± 120

Table 8: Electron identification efficiencies and QCD di-jet background rejections obtained for loose and medium identification cuts, including a calorimeter isolation cut (see text), and for three different jet E_T -ranges. The signal electrons are from $Z' \rightarrow e^+e^-$ decays with $m_{Z'}$ = 1 TeV and are required to have E_T > 100 GeV.

5 Electrons from $Z \rightarrow ee$ decays in early data

The experimental uncertainty on the electron identification efficiency is expected to be the source of one of the main systematic errors in many measurements, and in particular in cross-section determinations. In addition, a reliable monitoring of the electron identification efficiency is important in the commissioning phase of the detector and software. The previous sections have shown detailed estimates of the expected electron identification efficiency based on simulated samples. This section focuses on the measurement of electron reconstruction and identification efficiencies using a data-driven approach based on $Z \rightarrow ee$ events.

The tag-and-probe method [18] is used in this analysis. It consists of tagging a clean sample of events using one electron, and then measuring the efficiency of interest using the second electron from the Z-boson decay. Although more difficult because of trigger-threshold issues and of more severe background conditions, the same approach could be applied to J/ψ and Υ resonances, thus covering the lower end of the p_T spectrum [7].

5.1 Tag-and-probe method

The tag condition typically requires an electron identified with tight cuts. Both electrons are also required to be above a p_T threshold consistent with the trigger used. The invariant mass of the lepton pair is then used to identify the number of tagged events, N_1 (containing $Z \rightarrow ee$ decays), and a sub-sample N_2, where the second pre-selected electron further passes a given set of identification cuts. The efficiency for a given signature is given by the ratio between N_2 and N_1.

To account for background, the lepton-pair invariant mass spectrum is fitted around the Z mass peak using a Gaussian distribution convoluted with a Breit-Wigner plus an exponential function. The dominant background arises from QCD and is estimated using a procedure explained in [18]; its contribution is small in general and its impact on the measurement is therefore very limited.

The probe electron is checked against the selection as an electron candidate (to which only the pre-selection cuts are applied), and as a loose, medium or tight electron. To monitor in detail the efficiency dependence, the results are presented in bins of η and p_T , at the expense of an increased statistical error in each bin.

A quantitative comparison between the efficiency computed with this tag-and-probe method (ε_{TP}) and the efficiency obtained from the Monte Carlo truth (ε_{MC}) is used to validate the tag-and-probe method.

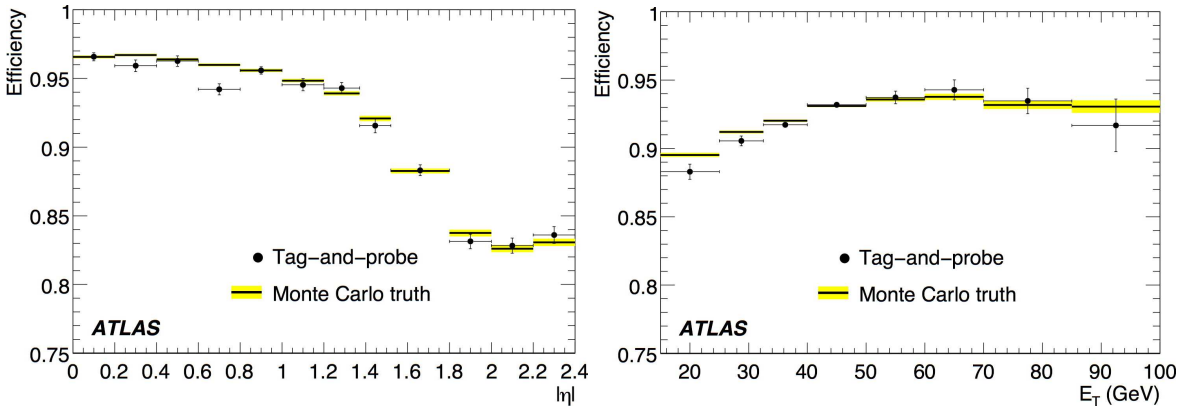

Figure 15: Efficiency of the electron pre-selection as a function of $|\eta|$ (left) and E_T (right) for $Z \rightarrow ee$ decays, using the tag-and-probe method and the Monte Carlo truth information.

E_T-range (GeV)	$15-25$		$25-40$		$40-70$	
$\|\eta\|-$range	ε_{TP}	$\Delta\varepsilon_{TP/MC}$	ε_{TP}	$\Delta\varepsilon_{TP/MC}$	ε_{TP}	$\Delta\varepsilon_{TP/MC}$
$0-0.80$	96.1±0.4	2.0±0.4	96.2±0.2	0.1±0.2	99.0±0.1	2.0±0.1
$0.80-1.37$	94.9±0.6	1.5±0.6	96.0±0.2	1.6±0.2	95.1±0.2	-0.5±0.2
$1.52-1.80$	89.0±1.2	3.6±1.2	88.8±0.6	1.3±0.6	91.9±0.6	1.7±0.6
$1.80-2.40$	83.0±1.0	0.6±1.0	83.2±0.6	0.8±0.6	84.9±0.6	1.1±0.6

Table 9: Efficiency of the electron pre-selection, ε_{TP}, in percent as obtained from the tag-and-probe method, for different ranges of electron E_T and $|\eta|$. The errors quoted for ε_{TP} are statistical and correspond to an integrated luminosity of 100 pb^{-1} . Also shown is the difference, $\Delta\varepsilon_{TP/MC}$, between this estimate of the pre-selection efficiency and that obtained using the matching to the Monte Carlo electron.

5.2 Electron reconstruction efficiency

The reconstruction and identification of electrons is based on seed-clusters in the electromagnetic calorimeter matched to tracks, as explained in Section 2. The tag electron is a reconstructed electron selected using tight (isol) cuts and also required to pass the trigger EM13i/e15i [11]. The tag electron is also required to be outside the barrel/end-cap transition region ($1.37 < |\eta| < 1.52$). The probe electron is pre-selected by identifying a cluster in the opposite hemisphere, such that the azimuthal difference between tag and probe electrons is $\Delta\phi > 3/4\pi$. Both tag and probe electrons are required to have E_T >15 GeV. The invariant mass of the lepton pair is required to be between 80 and 100 GeV. Figure 15 compares ε_{TP} and ε_{MC} as a function of $|\eta|$ and E_T . Table 9 summarises the results obtained for this first step in the reconstruction and identification of the probe electron.

5.3 Electron identification efficiency.

In this section, the electron identification efficiency is presented with respect to the reconstructed electrons discussed in Section 5.2. The QCD background was not considered here, since it is less than a few percent below the Z-boson mass peak. The reconstructed probe electron was checked against loose, medium and tight selection cuts. Table 10 summarises the results obtained for this second step in the reconstruction and identification of the probe electron. Figure 16 shows as a function of η and p_T the

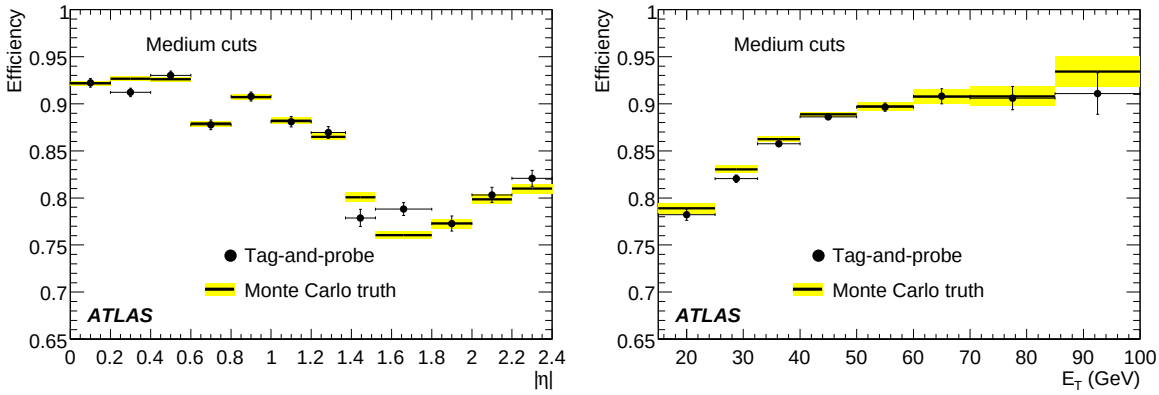

Figure 16: Efficiency of the medium electron identification cuts relative to the pre-selection cuts as a function of $|\eta|$ (left) and E_T (right) for $Z \rightarrow ee$ decays, using the tag-and-probe method and the Monte Carlo truth information.

comparison between ε_{TP} and ε_{MC}, for the medium cuts. The losses at high η are due to the material in the inner detector, as discussed in Section 2.

5.4 Statistical and systematic uncertainties

A number of uncertainties may affect these tag-and-probe measurements once the accumulated data will provide high enough statistics to perform similar measurements to those quoted above:

- Differences between ε_{TP} and ε_{MC}
  The relative difference $\Delta\varepsilon_{TP/MC}$ in regions (in p_T and $|\eta|$), where the efficiency is flat, is less than 0.5%, assuming that the statistical error on ε_{MC} is negligible. $\Delta\varepsilon_{TP/MC}$ marginally depends on the definition of a true electron and the systematic uncertainty related to this is estimated to be $< 0.1\%$, when varying the cut on the separation in η/ϕ space (ΔR) between the reconstructed electron candidate and the true electron.

- Statistical uncertainty.
  The size of the available Z-boson sample is a source of systematic error. With an integrated luminosity of 100 pb^{-1} , the error is expected to be in the range 1-2% for $p_T > 25$ GeV, and $\sim 4\%$ in the low-p_T bin.

- Selection criteria
  Another source of systematic error comes from varying the selection criteria. For instance, uncertainties introduced by varying the cut on the Z-boson mass or requiring an isolation criterion for the probe electron were evaluated. The magnitude of the uncertainty introduced is smaller than 0.5% for $p_T > 40$ GeV. At low p_T , this uncertainty is estimated to be in the 1-2% range.

- QCD background contribution
  Adding the expected contribution from the QCD background to the signal does not degrade the results, except for $1.52 < |\eta| < 1.8$, a region which is close to the barrel/end-cap transition region and also where the efficiency is not uniform. The contribution from the uncertainties on the residual QCD background is expected to be negligible.

Loose	$15-25$		$25-40$		$40-70$	
$\lvert\eta\rvert \backslash p_T$	ε_{TP}	$\Delta\varepsilon_{TP/MC}$	ε_{TP}	$\Delta\varepsilon_{TP/MC}$	ε_{TP}	$\Delta\varepsilon_{TP/MC}$
$0-0.8$	95.2 ± 2.0	-4.1 ± 2.0	98.8 ± 0.3	-0.5 ± 0.3	99.8 ± 0.1	0.2 ± 0.1
$0.8-1.37$	92.3 ± 2.1	-6.9 ± 2.1	98.9 ± 0.3	-0.7 ± 0.3	99.6 ± 0.2	0.0 ± 0.2
$1.52-1.8$	100.0 ± 2.8	1.7 ± 2.8	99.4 ± 0.5	0.0 ± 0.5	99.6 ± 0.5	0.0 ± 0.5
$1.8-2.4$	98.8 ± 1.6	0.6 ± 1.7	98.8 ± 0.5	0.0 ± 0.5	99.1 ± 0.4	-0.2 ± 0.4

Medium	$15-25$		$25-40$		$40-70$	
$\lvert\eta\rvert \backslash p_T$	ε_{TP}	$\Delta\varepsilon_{TP/MC}$	ε_{TP}	$\Delta\varepsilon_{TP/MC}$	ε_{TP}	$\Delta\varepsilon_{TP/MC}$
$0-0.8$	83.6 ± 2.3	-4.3 ± 2.7	89.7 ± 0.7	-0.8 ± 0.8	92.6 ± 0.5	-0.2 ± 0.6
$0.8-1.37$	75.6 ± 2.8	-7.5 ± 3.4	87.6 ± 0.9	0.7 ± 1.0	90.9 ± 0.8	-0.4 ± 0.8
$1.52-1.8$	71.9 ± 4.4	5.9 ± 6.5	76.9 ± 1.9	-2.2 ± 2.4	83.6 ± 1.9	0.7 ± 2.3
$1.8-2.4$	78.0 ± 2.7	6.5 ± 3.7	79.2 ± 1.4	1.7 ± 1.8	82.5 ± 1.4	-1.0 ± 1.6

Tight	$15-25$		$25-40$		$40-70$	
$\lvert\eta\rvert \backslash p_T$	ε_{TP}	$\Delta\varepsilon_{TP/MC}$	ε_{TP}	$\Delta\varepsilon_{TP/MC}$	ε_{TP}	$\Delta\varepsilon_{TP/MC}$
$0-0.8$	68.7 ± 2.6	-5.2 ± 3.5	73.8 ± 1.0	-1.2 ± 1.3	77.0 ± 0.9	-1.5 ± 1.1
$0.8-1.4$	61.8 ± 3.0	-3.1 ± 4.7	72.9 ± 1.2	0.7 ± 1.7	77.3 ± 1.1	0.2 ± 1.5
$1.5-1.8$	55.7 ± 4.5	6.8 ± 8.6	65.9 ± 2.1	-0.8 ± 3.1	73.7 ± 2.2	1.2 ± 3.1
$1.8-2.4$	66.2 ± 3.0	8.5 ± 4.9	66.0 ± 1.6	2.6 ± 2.5	73.4 ± 1.6	0.7 ± 2.2

Table 10: Loose, medium and tight electron identification efficiencies relative to the pre-selection efficiencies for different bins in E_T and $|\eta|$. The first error is statistical and corresponds to an integrated luminosity of 100 pb^{-1} . The second error is the difference obtained between ε_{TP} and ε_{MC}.

6 Conclusion

Excellent electron identification will clearly play an important role at the LHC, since high-p_T leptons will be powerful probes for physics within and beyond the Standard Model. Based on this motivation, various algorithms and tools have been developed to efficiently reconstruct and identify electrons and separate them from the huge backgrounds from hadronic jets.

Presently, two reconstruction algorithms have been implemented in the ATLAS offline software, both integrated into one single package and a common event model. The first one relies on calorimeter seeds for reconstructing electrons, whereas the second algorithm relies on track-based seeds, is optimised for electrons with lower energies, and relies less on isolation.

The calorimeter based algorithm starts from the reconstructed cluster in the electromagnetic calorimeter, then builds identification variables based on information from the calorimeter and the inner detector. The rejection power with respect to QCD jets comes almost entirely from the identification procedure. Depending on the electron transverse energy and the analysis requirements, rejection factors of 500 to 100 000 can be achieved, for efficiencies of 88% to 64%, using a simple cut-based selection. More refined identification procedures combining calorimeter and track quantities using multivariate techniques provide a gain in rejection of about $20-40\%$ with respect to the cut-based method, for the same efficiency of $61-64\%$. Alternatively, they provide a gain of $5-10\%$ in efficiency, for the same jet rejection (tight and medium cuts).

Electrons in the forward region can also be identified and separated from the background. A simple cut-based method, exploring the energy depositions in the inner wheel of the electromagnetic end-cap calorimeter and in the forward calorimeter as well as the shower-shape distributions, shows that $\sim 99\%$ of the QCD background can be rejected, for an electron identification efficiency of $\sim 80\%$. This per-

formance should be sufficient to select cleanly, for example, $Z \rightarrow ee$ decays with one electron in the forward region.

Studies of the strategies for measuring efficiencies and fake rates in early data show that the tag-and-probe method is a good tool to estimate the electron identification efficiency and to control the reliability of the Monte Carlo simulation. With 100 pb^{-1} , the method is limited by the statistics of the Z sample, whereas its systematic uncertainty is of the order of 1 to 2 %.

The work presented here primarily addresses the description and performance of the offline reconstruction and identification of electrons. However, it also gives an overview of the possible path towards physics discoveries with electrons in Higgs, SUSY, and exotic scenarios.

References

[1] ATLAS Collaboration, Detector and Physics Technical Design Report, Vol.1, CERN/LHCC/99-14 (1999).

[2] ATLAS Collaboration, G. Aad et al., The ATLAS experiment at the CERN Large Hadron Collider, 2008 JINST 3 S08003 (2008).

[3] ATLAS Collaboration, Calibration and Performance of the Electromagnetic Calorimeter, this volume.

[4] ATLAS Electromagnetic Liquid Argon Calorimeter Group, B. Aubert et al., Nucl. Inst. Meth. A500 (2003) 202-231.

[5] ATLAS Electromagnetic Liquid Argon Calorimeter Group, B. Aubert et al., Nucl. Inst. Meth. A500 (2003) 178-201.

[6] ATLAS Electromagnetic Barrel Calorimeter, M. Aharrouche et al., Nucl. Inst. Meth. A568 (2006) 601-623.

[7] ATLAS Collaboration, Reconstruction of Low-Mass Electron Pairs, this volume.

[8] K. De, ATLAS Computing System Commissioning-Simulation Experience, and R. Jones, Summary of Distributed data analysis and information management, Proceedings of the 16^{th} International Conference on Computing and In High Energy and Nuclear Physics (2007).

[9] ATLAS Collaboration, Liquid Argon Calorimeter Technical Design Report, CERN/LHCC/96-41(1996).

[10] T. Sjostrand, S. Mrenna and P. Skands, FERMILAB-PUB-06-052-CD, JHEP 0605:026 (2006).

[11] ATLAS Collaboration, Physics Performance Studies and Strategy of the Electron and Photon Trigger Selection, this volume.

[12] GEANT4 Collaboration, Geant4 - A simulation toolkit, Nuclear Instruments and Methods in Physics Research Section A 506 (2003) 250-303.

[13] W. Lampl et al., Calorimeter Clustering Algorithms: Description and Performance, ATLAS-LARG-PUB-2008-002 (2008).

[14] ATLAS Collaboration, Forward-Backward Asymmetry in $pp \rightarrow Z/\gamma^{\star} \rightarrow e^{+}e^{-}$ Events, this volume.

[15] ATLAS Collaboration, Search for the Standard Model $H \rightarrow ZZ^{*} \rightarrow 4l$, this volume.

[16] ATLAS Collaboration, Prospects for Supersymmetry Discovery Based on Inclusive Searches, this volume.

[17] ATLAS Collaboration, Dilepton Resonances at High Mass, this volume.

[18] CDF Collaboration, First measurements of inclusive W and Z cross sections from Run II of the Fermilab Tevatron Collider, Phys. Rev. Lett. 94, 091803 (2005);
D0 Collaboration, Measurement of the shape of the boson rapidity distribution for $p\bar{p} \rightarrow Z/\gamma^{\star} \rightarrow e^{+}e^{-} + X$ events produced at $\sqrt{s}$ of 1.96 TeV, hep-ex/0702025 (2007).

[19] ATLAS Collaboration, Electroweak Boson Cross-Section Measurements, this volume.